Research in Astronomy and Astrophysics, 23:095003 (9pp), 2023 September https://doi.org/10.1088/1674-4527/acdfa6

Multimodality-based Wind Speed Forecasting Method for the Wind Resistance Control of Large Radio Telescope

Wen-Juan Wang[1], Bao-Qing Han[1,6], Long-Yang Wang[1], Tian Luan[1], Yue-Fei Yan[1,6], Wu-Lin Zhao[2], De-Qing Kong[3], Yang Wu[4], and Cong-Si Wang[5]

[1] Key Laboratory of Electronic Equipment Structure Design, Ministry of Education, Xidian University, Xi'an 710071, China; hanbaoqing18@163.com, yfyan530@163.com

[2] The 39th Research Institute of China Electronics Technology Group Corporation, Xi'an 710065, China

[3] National Astronomical Observatories, Chinese Academy of Sciences, Beijing 100101, China

[4] The 54th Research Institute of China Electronics Technology Group Corporation, Shijiazhuang 050081, China

[5] Guangzhou Institute of Technology, Xidian University, Guangzhou 510555, China

Received 2023 April 10; revised 2023 May 25; accepted 2023 June 15; published 2023 July 31

Abstract

A large, fully steerable radio telescope is susceptible to the wind load, leading to structure deformation and pointing deviation of the telescope. To effectively suppress the influence of dynamic wind load, the wind resistance control of the telescope is carried out based on wind speed forecasting. This study developed a wind speed forecasting model to efficiently forecast the wind speed at the telescope position. The proposed model successfully eliminates the random noise of the original wind speed, effectively extracts the wind speed features and solves the automatic optimization of the hyperparameters of the forecasting network. This model significantly improves the accuracy and reliability of wind speed forecasting. To verify the forecasting performance of the proposed model, the wind data from the Qitai Radio Telescope site is examined as a case study. The wind speed forecasting model's MAE, RMSE and MAPE are 0.0361, 0.0703 and 3.87%, respectively. The performance of the proposed model meets the requirements of wind resistance control and can provide data support for the radio telescope.

Key words: telescopes – methods: numerical – methods: data analysis

1. Introduction

Radio telescopes are widely used in radio astronomy, satellite communication, deep space exploration and other fields. The larger the effective aperture of the telescope is, the higher the gain (Haupt & Samii 2015). The construction of a larger radio telescope is the main way to improve its performance. China intends to build the 110m Qitai Radio Telescope (QTT) in Qitai, Xinjiang (Wang 2014). However, an increase in the telescope aperture would lead to the narrowing of the antenna beam, so the requirement of antenna pointing accuracy is higher (Wang et al. 2019). At the same time, the huge windward surface leads to a decrease in the structural stiffness of the telescope, which makes the influence of wind disturbance on the telescope more serious (Zhang et al. 2015). It is urgent to develop an effective compensation method for the wind disturbance problem of radio telescopes to suppress the wind disturbance.

In reducing the influence of wind disturbance on radio telescopes, engineers usually use a servo control system to compensate for the structural deformation a telescope. Currently, many telescope systems mainly employ the PID algorithm for servo control (Qiu et al. 2014). However, the PID algorithm is unable to actively compensate for wind disturbances that affect the telescope's performance. Therefore, many studies have designed new wind disturbance rejection servo controllers and control algorithms to improve the disturbance rejection ability of the servo system (Sun et al. 2013; Zhang & Liao 2013). The wind load acting on the antenna system is difficult to measure directly, and it is impossible to fully compensate the influence on the antenna even through system modeling. After the current wind information is measured, servo control is used to correct the pointing of the antenna (Yan et al. 2022). However, the wind undergoes instantaneous changes in a time-varying manner, but the servo control system has a time delay, making it difficult for the servo control system of the radio telescope to perform adjustments (Lian et al. 2021). It is urgent to study a method to enhance the pointing control of radio telescopes in real-time. Therefore, a wind resistance control strategy based on wind speed forecasting is proposed. We rely on historical data to establish a wind speed forecasting model to obtain wind speed information at the antenna position in advance. Obtaining wind speed information in advance provides sufficient calculation and response time for the servo control system of the telescope. Wind speed forecasting realizes the radio telescope's active

[6] Corresponding authors.

wind resistance control strategy in the time-varying wind environment (Gawronski et al. 2004).

At present, wind speed forecasting models could be divided into physical models based on the wind mechanism, time series models based on historical data and artificial intelligence models based on a multi-layer perceptron according to the method of building the model (Soman et al. 2010; Chang 2014). The physical model considers atmospheric boundary layer theory, fluid mechanics theory and micrometeorology theory. It explains the formation mechanism of wind and forecasts wind speed by simulating the entire wind formation process (Zhao et al. 2016). This kind of model generates high accuracy, such as numerical weather prediction (NWP). The time series model mainly establishes a mapping relationship between the historical data of wind speed and future data. Based on the past wind speed data, a regression model is established to forecast the wind speed so as to avoid incorporating the complex formation mechanism of wind, and is widely used in short-term wind speed forecasting applications (Han et al. 2017). Commonly applied methods include autoregressive moving average (ARMA) and exponential smoothing (ES) (Huang et al. 2021). The complex neural network structure of the artificial intelligence model can well capture the nonlinear relationship between the historical wind speed data. The neurons in the network enable the learning ability for the model. The artificial intelligence model can actively learn the complex mapping relationship between input and output, which has strong information synthesis ability and strong robustness (Gan et al. 2021), such as in a recurrent neural network (RNN) and convolutional neural network (CNN).

However, the above forecasting models have inherent defects, summarized as follows. Modeling a physical process is complex. Moreover, it requires a lot of operation time and computing resources. A time series model is poor at dealing with fluctuating and non-stationary data. Artificial intelligence models are prone to fall into a local optimum or overfitting. Each model has unavoidable limitations. The conventional forecasting model ignores the importance of data feature extraction. Wind speed has nonlinear and non-stationary characteristics. Data preprocessing can improve the data quality. If we use the original wind speed to model directly, there will be many errors, leading to the model's poor forecasting ability (Liu et al. 2021).

Therefore, we combine data preprocessing with the wind forecasting algorithm. A combined wind speed forecasting model based on data processing is proposed in this study. The model includes a data decomposition strategy, an advanced optimization algorithm and a deep learning algorithm. Overall, we obtain an effective combined wind speed forecasting model. The forecasting model is simulated and tested based on the wind speed data of the QTT site. The results show that the forecasting model can effectively improve accuracy and reliability. The intelligent wind speed forecasting model can provide strong technical support for the wind resistance control of large radio telescopes.

Radio telescopes require stable pointing control to obtain accurate observation data. However, wind loads can impact telescope observations, thereby affecting the quality of the data obtained (Li et al. 2022). Therefore, we apply wind forecasting technology to the field of radio telescopes to improve their stability and precision. We design a wind forecasting model suitable for radio telescopes, considering factors such as the structure and location of the telescopes, as well as the influence of wind speed. We have optimized the wind forecasting technology to improve its accuracy and reliability, ensuring the long-term stable operation of the radio telescope.

2. Methodology of Wind Speed Forecasting

In this section, the main modules used in the proposed forecasting system are discussed in detail: wind speed data decomposition, parameter optimization and the deep learning forecasting algorithm. The specific steps of the forecasting system are as follows:

2.1. Wind Speed Data Decomposition

The decomposition strategy transforms the nonlinear and non-stationary original wind speed into multiple components. The obtained wind speed components are stable and regular (Huang et al. 1998). We use improved complete ensemble empirical mode decomposition with adaptive noise (ICEEMDAN) to decompose wind speed. ICEEMDAN directly decomposes unknown signals into multiple components from high frequency to low frequency based on time domain features of signals (Colominas et al. 2014). ICEEMDAN decomposes the wind speed data into multiple modes, namely intrinsic mode function (IMF), which contains the characteristic information on the wind speed. The following summarizes the main processing steps:

1. Add the white Gaussian noise decomposed by empirical mode decomposition (EMD) to the original signal to construct the signal with noise $f_i(x)$, then sum the $f_i(x)$ to get the first-order residual R_1:

$$f_i(x) = f(x) + \varepsilon E_1\{w^{(i)}\}, \tag{1}$$

$$R_1 = M\{f_i(x)\}, \tag{2}$$

where $f(x)$ is original wind speed data, ε is the noise decomposition coefficient, w is the white noise added for the i_{th} time, $E\{\cdot\}$ represents the EMD operator, E_1 denotes the noise component obtained by the first EMD and $M\{\cdot\}$ represents the local mean operator.

2. The first IMF of the wind speed decomposition is obtained by subtracting the original data from the first

residual:

$$\mathrm{IMF}_1 = f(x) - R_1. \tag{3}$$

3. The second decomposition residual R_2 and the second IMF calculation formula are:

$$R_2 = M\{R_1 + \varepsilon E_2\{w^{(i)}\}\}. \tag{4}$$

$$\mathrm{IMF}_2 = R_1 - R_2. \tag{5}$$

4. The k_{th} decomposition residuals and the IMF_k are calculated as follows:

$$R_k = M\{R_{k-1} + \varepsilon E_k\{w^{(i)}\}\} \quad (k = 3, 4,\ldots). \tag{6}$$

$$\mathrm{IMF}_k = R_{k-1} - R_k \quad (k = 3, 4,\ldots). \tag{7}$$

5. Repeat (d) until the wind speed can no longer be decomposed, all wind speed components are obtained and the rest are residual components. The IMF and residual components obtained by ICEEMDAN are all the wind speed components of the wind speed decomposition. The wind speed components are used to establish the forecasting model

2.2. Parameter Optimization

Parameter optimization tries to optimize the hyperparameters of the neural network. The neural network's learning ability is limited. Appropriate network parameter settings can further improve the accuracy of the forecasting model. Harris hawks optimization (HHO) is a swarm intelligence optimization algorithm obtained by simulating a group of Harris hawks preying on prey, which can optimize multiple parameters in the target (Heidari et al. 2019).

HHO consists of two phases: global exploration and local exploitation. During the first phase, Harris hawks randomly roost in certain locations to detect prey. During the second phase, the Harris hawks start to surprise prey, and the prey starts to escape. Harris hawks have four hunting strategies: soft besiege, hard besiege, soft besiege with progressively rapid dives and hard besiege with progressively rapid dives. As shown below, r represents the escape probability, and E signifies the escape energy. The larger the E is, the stronger the prey's energy.

(i) Soft besiege. When $r \geqslant 0.5$, $E \geqslant 0.5$, the energy of the prey is high, and it is not easy for the Harris hawks to catch it. So, they would consume the physical strength of the prey first, and then gently siege the prey in the best position until they have exhausted their prey

$$\begin{aligned} X(t+1) &= X_p(t) - X(t) - E|JX_p(t) - X(t)| \\ &= \Delta X(t) - E|JX_p(t) - X(t)|, \end{aligned} \tag{8}$$

where $X(t+1)$ is the individual position at the next iteration, $X(t)$ is the current position of the individual, $X_p(t)$ is the prey position, which represents the individual position of the optimal fitness value, and $\Delta X(t)$ denotes the difference between the prey position and the individual position.

(ii) Hard besiege. When $r \geqslant 0.5$, $E < 0.5$, the prey is not strong enough to escape, and the Harris hawks directly launch the hard besiege

$$X(t+1) = X_p(t) - E|\Delta X(t)|. \tag{9}$$

(iii) Soft besiege with progressively rapid dives. When $r < 0.5$, $E \geqslant 0.5$, the prey has a chance to escape and the escape energy is sufficient, so it is not easy to be caught. Therefore, the Harris hawks will perform progressively rapid dives and soft besiege. Here, the Levy flight is used to simulate the escape and jumping process of the prey:

$$X(t+1) = \begin{cases} Y, & f(Y) < f(X(t)) \\ Z, & f(Z) < f(X(t)) \end{cases}, \tag{10}$$

$$Y = X_p(t) - E|JX_p(t) - X(t)|, \tag{11}$$

$$Z = Y + S \times \mathrm{LF}(D), \tag{12}$$

where D is the dimension, S denotes a D dimensional random vector element value between [0,1], $\mathrm{LF}(\cdot)$ represents the Levy flight function and $f(\cdot)$ signifies the fitness function.

(iv) Hard besiege with progressively rapid dives. When $r < 0.5$, $E < 0.5$, the prey has a chance to escape but the escape energy is low. In order to ensure that the prey could be caught, the Harris hawks perform progressively rapid dives and hard besiege:

$$X(t+1) = \begin{cases} Y, & f(Y) < f(X(t)) \\ Z, & f(Z) < f(X(t)) \end{cases}, \tag{13}$$

$$Y = X_p(t) - E|JX_p(t) - \overline{X(t)}|, \tag{14}$$

$$Z = Y + S \times \mathrm{LF}(D), \tag{15}$$

where $\overline{X(t)}$ is the average position of individuals in the population.

We optimized several hyperparameters of the neural network, including the number of neurons in the hidden layer, the learning rate and the number of training epochs. Applying the HHO algorithm helps the neural network to have a more suitable hyperparameter setting.

2.3. Deep Learning Algorithm

Bidirectional long short-term memory (BiLSTM) neural network features are suitable for wind speed time series forecasting. BiLSTM adds a layer of reverse long short-term memory (LSTM) neural network on the basis of LSTM. Bidirectional messaging allows BiLSTM to extract data information better. The output combination of forward and reverse LSTM is passed to the fully connected layer. Finally, the wind speed forecasting results are output after data dimension reduction. The weights and biases in the BiLSTM network are obtained through training. Other parameters in the network are set based on experience or take a long step to test appropriate parameter values. We use the neural network with optimized hyperparameters for modeling. The specific steps include initializing the parameters of the algorithm, setting the value range of the parameter to be optimized and training the neural network.

2.4. Model Evaluation Metrics

At present, there is no complete metric to evaluate the performance of the wind forecasting model (Xu et al. 2017). To quantitatively evaluate the forecasting model, five evaluation metrics are listed: mean absolute error (MAE), root mean square error (RMSE), mean absolute percentage error (MAPE), coefficient of determination (R^2) and sum of squared error (SSE). MAE is a measure of the deviation between the actual value and the predicted value. RMSE is more sensitive to outlier values and increases the penalty for the sample with large errors. MAPE is a measure of the relative deviation between the actual value and the predicted value, and it does not need to combine numerical dimensions to judge the difference. R^2 is used to judge the goodness of fit of the model. SSE is the overall error of the statistically predicted value. The calculation method of each evaluation metric is listed below:

$$\mathrm{MAE} = \frac{1}{n}\sum_{i=1}^{n}|y_i - \hat{y}_i|, \tag{16}$$

$$\mathrm{RMSE} = \sqrt{\frac{1}{n}\sum_{i=1}^{n}(y_i - \hat{y}_i)^2}, \tag{17}$$

$$\mathrm{MAPE} = \frac{1}{n}\sum_{i=1}^{n}\left|\frac{y_i - \hat{y}_i}{y_i}\right| \times 100\%, \tag{18}$$

$$R^2 = 1 - \frac{\sum_{i=1}^{n}(y_i - \hat{y}_i)^2}{\sum_{i=1}^{n}(y_i - \bar{y})^2}, \tag{19}$$

$$\mathrm{SSE} = \sum_{i=1}^{n}(y_i - \hat{y}_i)^2, \tag{20}$$

where n is the number of samples, y_i is the actual value of the wind speed, $\hat{y}_i$ denotes the predicted value of the wind speed and $\bar{y}$ represents the average value of the wind speed.

2.5. Proposed Forecasting System

Based on the abovementioned algorithm, we developed a wind speed forecasting model implementing a multiple-component ensemble. It integrates the data decomposition strategy, parameter intelligent optimization method and deep learning algorithm. The major steps are listed below, and the flowchart is presented in Figure 1.

Step 1: Data decomposition

The complex original wind speed data are decomposed and transformed into several simple wind speed components, thereby removing high-frequency noise and random interference. ICEEMDAN decomposes wind speed data into multiple components, then reconstructs the wind speed with noise filtering. At the same time, each wind speed component contains different features of the original wind speed, and this feature extraction is helpful for wind speed forecasting.

Step 2: Construction of the forecasting model

In order to obtain the optimal hyperparameters of the deep learning algorithm BiLSTM, a method for automatically optimizing neural network hyperparameters, was developed based on HHO. Initialize the parameters of BiLSTM and HHO first. HHO iterative optimization obtains the parameter group with the best fitness and builds the BiLSTM forecasting model based on these parameters. HHO has fewer variables, fast convergence speed and strong global search ability. It is suitable for integration with neural networks and performs well in the process of optimizing network hyperparameters.

Step 3: Wind speed forecasting

The proposed model applies the single-step rolling forecasting mechanism. The wind speed component after data preprocessing is input into the forecasting model. The first prediction value is obtained from the actual value in front of it. The time step is advanced by one step. The next prediction value is obtained from the actual value in front of it, and so on, using actual historical data to forecast all future data step by step. The final wind speed forecasting results are the predicted values of integrating all wind speed components.

Step 4: Performance evaluation

In order to quantitatively evaluate and compare the performance of the proposed forecasting model with other models, five performance evaluation metrics are selected, namely MAE, RMSE, MAPE, R^2 and SSE. The metrics of RMSE, MAE and MAPE are calculations of the error of sample points. R^2 is used to measure the fitting effect between the predicted value and the real value. SSE sums the square of the error of each sample point.

3. Model Validation and Results Analysis

To verify the validity of the proposed forecasting model, we took the wind data of the QTT site as an example to conduct a case study. First, the wind speed is decomposed into multiple modes based on the decomposition strategy, eliminating the negative impact of high-frequency noise and extracting the wind speed feature. Data preprocessing reduces uncertainty and volatility of wind speed. Then the advanced intelligent algorithm HHO was used to optimize the parameters of the neural network automatically. Finally, we use the wind speed modes obtained from the decomposition strategy to train the forecasting model. The forecasting results are reconstructed to get the wind speed forecasting results. The forecasting performance of these models is comprehensively evaluated with five effective evaluation metrics. The forecasting accuracy of the proposed model is compared and analyzed with nine other models.

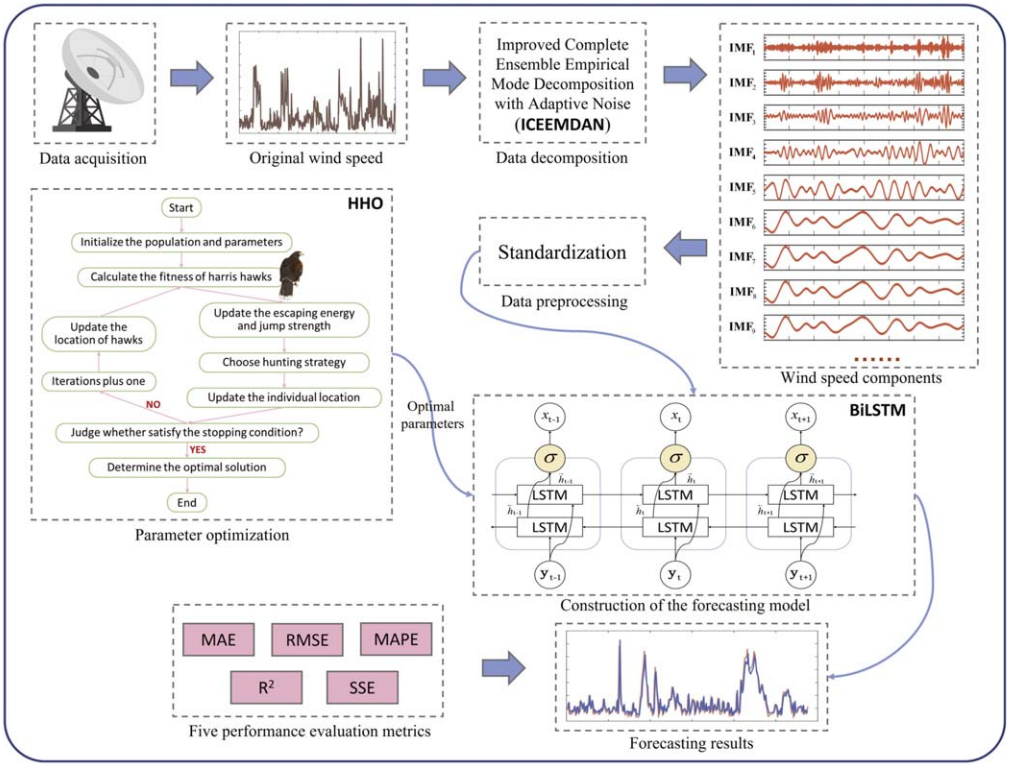

Figure 1. Flowchart of the forecasting system.

Figure 2. The site of QTT.

3.1. Wind Field Datasets

The data set used comes from the wind tower on the QTT site. The site is located in Qitai, Xinjiang, which is a rectangular basin with a distance of about 1.5 km from east to west and about 2 km from north to south, surrounded by mountains (He et al. 2021). A wind measuring tower was built near the northwest of QTT, as illustrated in Figure 2. The wind speed and direction data of the QTT site for nearly a year were collected to obtain the wind rose diagram in Figure 3. It can be seen that the main wind direction of the site is the southeast and northwest, and the wind speed is not high in most cases.

The time interval of the wind speed data is 10 minutes. Since the future wind speed is related to the wind speed in a short period of time in the past, the network parameters of the forecasting model must be continuously learned and updated. We selected the wind speed data for ten days. The data from the first eight days were used as the training set, and the data from the last two days were utilized as the test set. The statistical

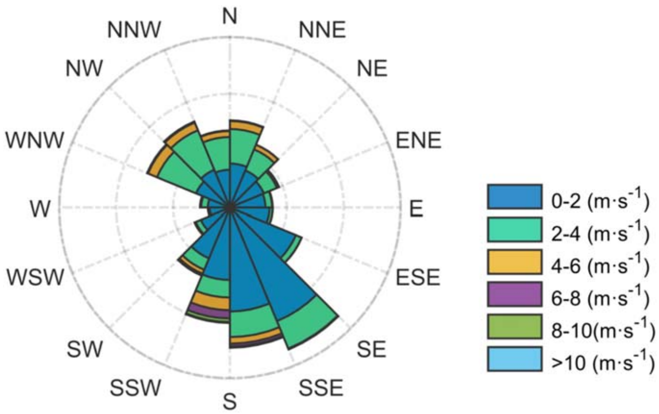

Figure 3. Wind rose diagram.

indicators (mean, maximum, minimum, standard deviation, skewness and kurtosis) of the wind speed data sets are shown in Table 1.

Among them, skewness and kurtosis are dimensionless, and the units of other indicators are meters per second. Skewness describes the degree to which the data distribution deviates from symmetry. The larger the skewness is, the more biased the probability distribution of the data set. Kurtosis describes the degree of the peak of the data distribution. The greater the kurtosis is, the higher and sharper the probability distribution of the data set.

3.2. Forecasting Results and Discussion

First, we performed an ICEEMDAN decomposition of the wind speed signal. Several groups of white noise are added to the wind speed signal to be decomposed, and the standard deviation of each noise group is 0.05 times the standard deviation of the wind speed signal. After the sequence is constructed, 50 averaging operations are performed on each group of residuals to obtain the first residual. Subtracting this residual from the wind speed signal gives the first IMF. The above steps are repeated until the two IMF constraints are satisfied, with the maximum number of sifting iterations allowed being 100. Finally, the wind speed signal is decomposed into several IMFs and a residual. Second, we introduce the HHO algorithm to optimize the number of neurons of the two hidden layers of the neural network, the maximum epoch and the initial learning rate. These four hyperparameters are randomly initialized. Based on experience, the lower and upper bounds of the variables are set to [10, 10, 100, 0.005] and [300, 300, 800, 0.05] respectively. We define the fitness function for evaluating the performance of each set of hyperparameter combinations as the loss function MSE of the neural network, searching for the minimum value of the fitness function in the target domain to obtain the optimal solution of the variable. Here, the neural network is built separately from the normalized wind speed components. Finally, we build the neural network forecasting model with the optimal solution of the hyperparameters.

The original wind speed is decomposed by the ICEEMDAN strategy to obtain ten IMFs, namely 10 wind speed components, as shown in Figure 4. The wind speed components are arranged according to the frequency from high to low, and the frequency of components decreases from left to right.

The ARMA model is a classic time series forecasting model, which is widely used in various time series forecasting. The back propagation neural network (BPNN) is a classic neural network model. ARMA and BPNN are typical representatives of linear and nonlinear models, respectively. Often regarded as a benchmark for wind speed forecasting to compare models, RNN is the mainstream neural network model for sequence data. Its three variants are LSTM, gated recurrent unit (GRU) and BiLSTM. The main difference between LSTM and GRU is the internal gating mechanism. The three gating units of LSTM can avoid the problems of gradient disappearance and gradient explosion during the model training process. GRU has only two gating units, and the model structure is simpler. BiLSTM works by inputting the input sequence into two LSTM layers from front to back and from back to front, and then splicing the outputs of the two LSTM layers. To compare the ICEEMDAN decomposition algorithm, we also introduce the empirical wavelet transform (EWT) decomposition algorithm to perform hybrid modeling of EWT with an individual model. EWT decomposes the data according to the frequency domain characteristics of the signal. EWT uses the signal itself to construct the wavelet basis function and converts the non-stationary signal into a time-frequency localized frequency component. We compared individual single models and four hybrid models with the proposed model. We calculated the error and goodness of fit for each model to evaluate the performance of the model.

Nine forecasting models (ARMA, BPNN, LSTM, GRU, BiLSTM, EWT-GRU, ICEEMDAN-GRU, EWT-BiLSTM and ICEEMDAN-BiLSTM) were compared with the proposed forecasting model, and the results are shown in Table 2. This table reports the forecasting results of the proposed model and other models. The units of MAE, RMSE and SSE are meters per second, meters per second and meter squared per second squared respectively. MAPE and R^2 are dimensionless. The bold numbers indicate that some evaluation metrics reflect better results than the others. Some conclusion can be drawn from it, that the proposed model has the best forecasting performance, and the values of MAE, RMSE, MAPE, R^2 and SSE are 0.0361, 0.0703, 3.87%, 0.9962 and 1.4217, respectively.

Compared to individual models (ARMA, BPNN, LSTM, GRU and BiLSTM), the MAE, RMSE, MAPE and SSE of the proposed model are significantly smaller. Among these individual models, the BiLSTM model has the highest

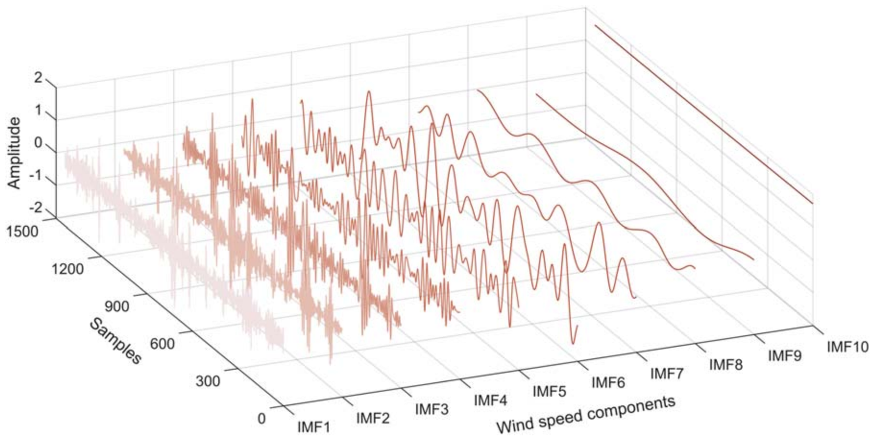

Figure 4. Wind speed components decomposed by ICEEMDAN.

Table 1
Statistical Indicators of Wind Speed Datasets

Sample	Number	Mean	Max	Min	Std	Skew	Kurt
All data	1440	1.601	8.43	0.111	1.273	1.594	5.738
Training set	1152	1.649	8.43	0.111	1.300	1.53	5.626
Test set	288	1.412	5.825	0.276	1.145	1.883	6.122

Table 2
Comparison of Forecasting Performance of Proposed Model and Other Models

Model	MAE	RMSE	MAPE	R^2	SSE
ARMA	0.4227	0.6011	42.21%	0.7233	104.0645
BPNN	0.4165	0.5903	41.25%	0.7331	100.3571
LSTM	0.4218	0.6030	41.95%	0.7215	104.7280
GRU	0.4129	0.5975	41.19%	0.7266	102.8077
BiLSTM	0.3393	0.4589	32.94%	0.8387	60.6451
EWT-GRU	0.2255	0.3487	23.03%	0.9069	35.0186
ICEEMDAN-GRU	0.1677	0.2256	18.34%	0.9610	14.6543
EWT-BiLSTM	0.0491	0.0910	5.23%	0.9937	2.3674
ICEEMDAN-BiLSTM	0.0455	0.0774	4.57%	0.9954	1.7237
Proposed model	0.0361	0.0703	3.87%	0.9962	1.4217

forecasting accuracy, and the values of MAE, RMSE, MAPE, R^2 and SSE are 0.3393, 0.4589, 32.94%, 0.8387 and 60.6451, respectively.

Four decomposition-based models are obtained by combining the two decomposition algorithms, EWT and ICEEMDAN, with two well-performing individual models, GRU and BiLSTM, respectively. In addition, when comparing the proposed model with the four decomposition-based models (EWT-GRU, ICEEMDAN-GRU, EWT-BiLSTM and ICEEMDAN-BiLSTM), the proposed model is still superior. Moreover, it can be concluded that the proposed model is excellent based on the performance metrics, which further verify that the proposed model is accurate and effective.

It can be observed that the actual wind speed value and the forecasted value of the proposed model and nine other models are plotted in Figure 5. Moreover, the decomposition-based models have basically the same trend as the actual value curve, but there are still some deviating points, while the proposed model fits the real value curve well. This affirms from another perspective that the proposed model has excellent forecasting performance.

The absolute error of each model is analyzed, as demonstrated in Figure 6. We use a boxplot to represent the absolute error of each model. The abscissa is the type of model, and ten models correspond to ten boxplots. The ordinate is the absolute error of the sample points of each model in meters per second. The solid line in the middle of the box is the median of the error. The upper and lower bounds of the box are the upper quartile Q3 and the lower quartile Q1 of the error, respectively. The upper solid line and the lower solid line outside the box are the upper and lower limits in the non-abnormal range of the error, respectively. The dots represent outliers signifying errors. The rule for determining outliers is that the error is greater than the upper quartile Q3. It can be seen that there are many outliers in other models, which indicate that there are many forecasted values with large deviations during the forecasting period of these models. At the same time, the upper edge of the boxplot for these models is higher, which shows that the average error of these models is more significant. The boxplot of the proposed model is the shortest, and the upper edge is the

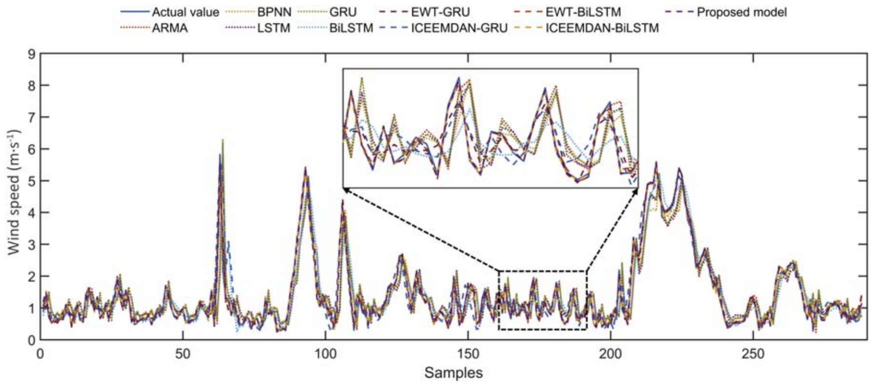

Figure 5. Comparison of forecasting results of the proposed model and other models.

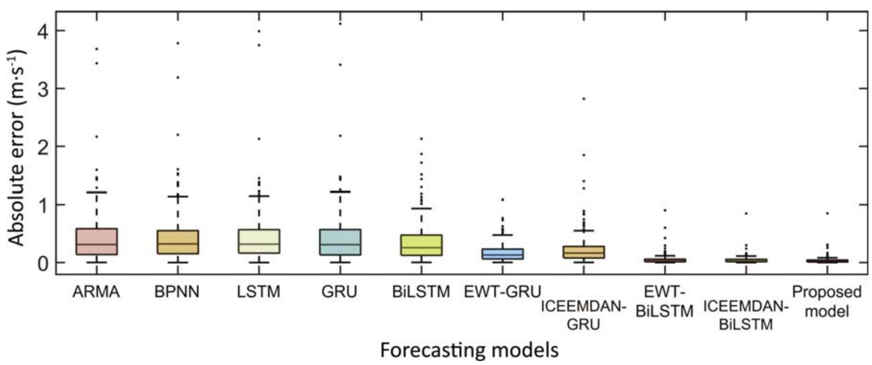

Figure 6. Absolute error of the proposed model and other models.

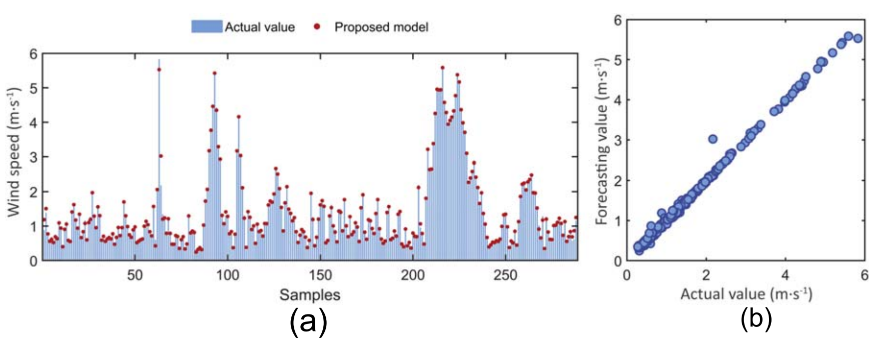

Figure 7. The forecasted results and scatter diagram of the proposed model. (a) Forecasted results of the proposed model; (b) Scatter diagram.

lowest. We can conclude that the proposed model is accurate and stable.

The forecasting results of the proposed model are further analyzed, as depicted in Figure 7. The cylinder and scatters in Figure 7(a) represent the actual value of wind speed and the forecasted value of the proposed model, respectively. The scatters in Figure 7(b) signify how well the forecasted value of wind speed corresponds to the actual value. It can be seen intuitively that the forecasted value almost totally agrees with the actual value. There are only apparent errors in some sudden changes in wind speed, and these errors are within acceptable limits.

The above experimental results can fully validate the effectiveness and accuracy of the proposed model. The proposed model has obvious performance improvement compared with other models. We use MAPE as the standard to calculate the improvement percentage of other models. The improvement percentages of these models, as listed previously, are 90.83%, 90.62%, 90.77%, 90.60%, 88.25%, 83.20%, 78.90%, 26.00% and 15.32%, respectively. Therefore, the proposed model's forecasting performance is superior to the other models, and it can achieve satisfactory forecasting accuracy.

4. Conclusions

This study successfully developed an intelligent wind speed forecasting model for wind resistance control. The model combines a data decomposition algorithm for eliminating interference and noise in wind speed, a data preprocessing technology for normalized data, and a group optimization algorithm for optimizing neural network parameters and comprehensive model evaluation criteria. We experimented using wind speed data provided by the QTT site as a case study to evaluate the performance of the developed model. Experimental results show that the developed model outperforms all other models. The proposed forecasting model effectively improves accuracy and adds a feasible direction for wind speed forecasting.

The wind speed forecasting accuracy of the proposed model is 96.13%, which meets the 90% accuracy requirement of wind resistance control. In practical application of the wind resistance control system, wind speed forecasting significantly improves the radio telescope's control efficiency. Accurate and stable wind speed forecasting can effectively reduce the pointing error of radio telescope observation caused by wind field uncertainty. The wind speed forecasting model can provide a time margin for the servo control system of the radio telescope by forecasting the wind speed in the following period and reserving sufficient time for the control system to compensate for the structural deformation. The wind speed forecasting combined with the servo control system guarantees the radio telescope's observation performance under wind disturbance. It is of great significance to the safety and stability of radio telescope operation.

Acknowledgments

This work was supported by the National Key Research and Development Program of China (grant No. 2021YFC2203600), National Natural Science Foundation of China (NSFC, grant No. 52275268), National Defense Basic Scientific Research Program of China (grant No. JCKY2021210B007), Wuhu and Xidian University Special Fund for Industry-University-Research Cooperation (grant No. XWYCXY-012021012), Youth Innovation Team of Shaanxi Universities (grant No. 201926), and Fundamental Research Funds for the Central Universities (grant No. XJSJ23122).

ORCID iDs

Wen-Juan Wang https://orcid.org/0000-0002-5106-2864

References

Chang, W. Y. 2014, J. Power Energy Eng., 02, 161
Colominas, M. A., Schlotthauer, G., Torres, M. E., et al. 2014, Biomed. Signal Process. Control., 14, 19
Gan, Z. H., Li, C. S., Zhou, J. Z., et al. 2021, Electr. Power Syst. Res., 191, 106865
Gawronski, W., et al. 2004, IAPM, 50, 58
Han, Q. K., Meng, H. M., Chu, F., et al. 2017, ECM, 148, 554
Haupt, R. L., & Samii, Y. R. 2015, IAPM, 57, 86
He, F. L., Xu, Q., Wang, N., et al. 2021, ChA&A, 118, 130
Heidari, A. A., Mirjalili, S., Faris, H., et al. 2019, Future Gener. Comput. Syst., 97, 849
Huang, N. E., Shen, Z., Long, S. R., et al. 1998, RSPSA, 454, 903
Huang, X. J., Wang, J. Z., Huang, B. Q., et al. 2021, ECM, 238, 114162
Li, L., Xu, Q., Wang, W. J., et al. 2022, AcASn, 63, 124, (in Chinese)
Lian, P. Y., Wang, C. S., Xue, S., et al. 2021, ENGINEERING-PRC, 7, 1047
Liu, M. D., Ding, L., Bai, Y. L., et al. 2021, ECM, 233, 113917
Qiu, D. M., Sun, M. W., Wang, Z. H., et al. 2014, IEEE Trans Control Syst Technol, 22, 1983
Soman, S. S., Zareipour, H., Malik, O., et al. 2010, in North American Power Symp. 2010 (Arlington, TX: Proc. IEEE), 1
Sun, M. W., Qiu, D. M., Wang, Y. K., et al. 2013, Optics and Precision Engineering, 21, 1568, (in Chinese)
Wang, C. S., Wang, X. Q., Xu, Q., et al. 2019, SCPMA, 130, 136, (in Chinese)
Wang, N. 2014, SCPMA, 44, 783 in Chinese
Xu, Y. Z., Yang, W. D., Wang, J. Z., et al. 2017, AtmEn, 148, 239
Yan, Y. F., Wang, C. S., Li, S., et al. 2022, SCPMA, 5, 22, (in Chinese)
Zhang, J., Huang, J., Qiu, L. L., et al. 2015, IAPM, 57, 6
Zhang, L., & Liao, X. J. 2013, Journal of South China University of Technology, 41, 22, (in Chinese)
Zhao, J. B., Guo, Z. H., Su, Z. Y., et al. 2016, ApEn, 162, 808